

See discussions, stats, and author profiles for this publication at: <https://www.researchgate.net/publication/268373989>

# Time-Dependent Structure and Solubilization Kinetics of Graphene Oxide in Methanol and Water Dispersions

ARTICLE *in* THE JOURNAL OF PHYSICAL CHEMISTRY C · NOVEMBER 2014

Impact Factor: 4.77 · DOI: 10.1021/jp506360f

---

CITATIONS

4

---

READS

39

# 1 Time-Dependent Structure and Solubilization Kinetics of Graphene 2 Oxide in Methanol and Water Dispersions

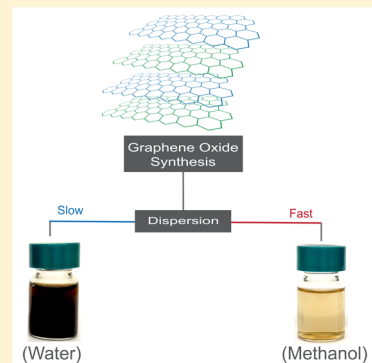
3 Flavio Pendolino,<sup>\*,†</sup> Emilio Parisini,<sup>‡</sup> and Sergio Lo Russo<sup>†</sup>

4 <sup>†</sup>Department of Physics and Astronomy, University of Padova, via Marzolo 8, 35131 Padova, Italy

5 <sup>‡</sup>Center for Nano Science and Technology @PoliMi, Istituto Italiano di Tecnologia, Via G. Pascoli 70/3, 20133 Milano, Italy

6  Supporting Information

7 **ABSTRACT:** Carbonaceous materials have long been attracting attention due to their  
8 physical and chemical properties as well as their low production costs. Among them,  
9 graphene oxide is considered to be an extremely promising material in the context of a  
10 wide spectrum of emerging technologies. However, since graphene oxide is characterized by  
11 a variable and therefore elusive chemical composition, complete control on the structure  
12 and the reactivity of this complex material has yet to be achieved, which clearly represents a  
13 knowledge gap that needs to be closed in order to confidently enable as many future  
14 applications as possible. Here, we present a spectroscopic study of graphene oxide  
15 obtained via the Sun method showing structural alteration of the material upon utilization  
16 of solvents of different polarity. In particular, our data provide clear experimental evidence  
17 that the use of methanol results in a graphene oxide material essentially enriched in  
18 carbonyl and hydroxyl groups. Moreover, the conjugated character of the material is also  
19 influenced by the nature of the solvent. The observed structural changes, which are due to  
20 the functionalization of the graphene basal plane, are time-dependent and correspond to  
21 different solubility properties of the resulting material. Finally, the modification of the graphene oxide structure alters the rate and  
22 the activation energy of solubilization.



## 23 ■ INTRODUCTION

24 Graphene oxide (GO) is attracting enormous attention as a  
25 graphene derivative material due to its remarkable physical  
26 properties and chemical features.<sup>1,2</sup> GO consists of a two-  
27 dimensional nanographene flake decorated with oxygen  
28 domains; while the graphene basal plane is essentially  
29 hydrophobic in nature, the oxygen atoms provide the material  
30 with a partial hydrophilic character. Basic structural differences  
31 between pristine graphene and GO relate to the material's  
32 carbon atom hybridization, which changes from  $sp^2$  to  $sp^3$  due  
33 to the binding of oxygen atoms to the graphene nanoflake.  
34 Over the past decade, the GO structure has been widely  
35 debated, and a number of structural models<sup>3–5</sup> have been  
36 proposed in connection with different synthetic procedures.<sup>6–10</sup>  
37 Moreover, it has been demonstrated that even the presence of  
38 contaminant amounts of heteroatoms from the starting  
39 reagents, such as sulfur atoms, or hole defects have significant  
40 effects on the properties and stability of the GO structure.  
41 Dimiev et al.<sup>11</sup> reported that GO structure undergoes  
42 modifications also when water is replaced by organic solvents  
43 during the purification process, supporting the notion that the  
44 functionalization of GO with specific chemical groups can, to a  
45 certain extent, be modified or tuned by means of an appropriate  
46 solvent selection. In fact, the major advantage of GO over  
47 pristine graphene is the possibility to functionalize the basal  
48 plane by relatively straightforward reactions in the liquid phase.  
49 Therefore, the presence of oxygen domains has profound  
50 implications in the reactivity of this material, which has raised

51 significant interest in a variety of technological areas such as  
52 conductive films,<sup>12</sup> hydrogen production,<sup>13</sup> energy storage  
53 systems,<sup>14</sup> organic emulsion solvents for industrial processes<sup>15</sup>  
54 or biosensors,<sup>16</sup> and water treatment.<sup>17</sup> Hence, it is important  
55 to acquire an in-depth knowledge of the chemical and physical  
56 properties of GO, particularly regarding the relationship  
57 between its structure, its kinetics of solubilization, and its  
58 chemical features. GO functionalization is critical with respect  
59 to the control and the modulation of the number and the  
60 nature of the specific chemical groups bonded on the graphene  
61 basal plane, which in turn affect the reactivity of the  
62 functionalized material. For example, Perreault et al.<sup>18</sup> showed  
63 that bacterial activity is inhibited when graphene oxide  
64 functionalized with  $C=O$  groups is used as a substrate.  
65 Currently, it is believed that GO dispersions are stable and that  
66 GO treatment with specific chemicals can lead to GO  
67 modifications.<sup>1,19–23</sup> Here, we provide experimental evidence  
68 that the GO structure can be modified and differentially  
69 functionalized by two factors: the *nature of the polar solvent used*  
70 and the *kinetics of the solubilization/dispersion process*. By  
71 comparing the modification of the functional groups on GO  
72 at various times, we show that the GO structure changes  
73 depending on the solvent in which GO is dispersed. Moreover,  
74 kinetic measurements were carried out in order to understand

Received: June 26, 2014

Revised: October 21, 2014

75 the solubilization process and its effects on the change of GO  
76 structure over time.

## 77 ■ EXPERIMENTAL SECTION

78 **Chemicals.** Expanded graphite ECOPHIT 50 was pur-  
79 chased from ECOPHIT.  $\text{KMnO}_4$ ,  $\text{H}_2\text{SO}_4$  (98%), and HCl  
80 (37%) were purchased from Sigma-Aldrich.

81 **Physicochemical Characterization.** Diffraction data were  
82 collected using a Bruker D8 Advance powder diffractometer  
83 with  $\text{Cu K}\alpha$  radiation ( $\lambda = 0.15418 \text{ nm}$ ). UV-vis spectra were  
84 recorded using a Jasco V/570 spectrometer and a quartz cell.  
85 FTIR measurements were carried out using a Jasco FT/IR-620  
86 spectrometer and KBr pellets.

87 **Synthesis of Graphene Oxide.** Graphene oxide was  
88 obtained using a modified Sun's synthetic protocol<sup>10</sup> to  
89 enhance safety conditions. Expanded graphite (5 g) and  
90 potassium permanganate (15 g) were introduced into a 1 L  
91 beaker and stirred until homogeneity. The beaker was placed in  
92 an ice–water bath, and 100 mL of concentrated sulfuric acid  
93 (98%) was added slowly (exothermic reaction) with continuous  
94 stirring until a petrol-green liquid paste was obtained. Then, the  
95 beaker was set to room temperature with a continuous stirring  
96 until a foam-like material was formed (about 20 min). At this  
97 stage, in order to improve safety, the foam material, which has  
98 density gradients, was stirred to homogeneity avoiding possible  
99 explosions when water is added (exothermic reaction). Thus,  
100 the beaker was placed again in the ice–water bath, and 400 mL  
101 of distilled water was added to it very slowly in order to avoid  
102 an uncontrolled temperature increase. The green-brownish  
103 liquid was then placed in the 90 °C water bath for 1 h to obtain  
104 a dark suspension. The suspension was paper filtered and  
105 washed first with 500 mL of distilled water, then with 200 mL  
106 of HCl 5%, to remove manganese, and finally again with 500  
107 mL of distilled water. The presence of sulfate ions in the GO  
108 dispersions was tested by a  $\text{BaSO}_4$  spot test.

109 **In Situ UV-vis Sample Preparation.** The GO dispersions  
110 were prepared in the quartz cell using 7 mg of GO and 3.5 mL  
111 of solvent. Gentle shaking was done by hand for about 5 min  
112 before measurements were recorded.

## 113 ■ RESULTS AND DISCUSSION

114 The synthesis of GO was done by means of a modification of  
115 the Sun's method.<sup>10</sup> The resulting filtrate was then divided into  
116 three flasks (30 mg of GO/7 mL of solvent) and dispersed in  
117 methanol (GO-Met), distilled water (GO-H<sub>2</sub>O), and 1:1  
118 methanol/water (GO-Mix), respectively. Subsequently, each  
119 of these samples was initially stirred for about 5 min and then  
120 left unshaken for about 2 h, to allow complete sedimentation of  
121 the floating particles. The final pH values after dispersion of  
122 GO are pH = 7 (GO-Met), pH = 3–4 (GO-H<sub>2</sub>O), and pH =  
123 6–7 (GO-Mix), respectively. As reported by Sun et al.,<sup>10</sup> the  
124 formation of a monolayer of GO is supported by a peculiar X-  
125 ray spectrum, in comparison with graphite. Powder X-ray  
126 diffraction analysis was carried out on the dried filtrates  
127 obtained from the GO-H<sub>2</sub>O, GO-Mix, and GO-Met  
128 dispersions (Figure 1). The expanded graphite pattern, which  
129 is reported as a reference, shows its characteristic narrow  
130 diffraction peak at  $2\theta = 26.5^\circ$  (main diffraction peak). The  
131 three different GO dispersions all show a peak centered at  
132  $11.2^\circ$ . These values are associated with the variation of the GO  
133 interlayer distance ( $d = 0.8 \text{ nm}$ ) due to the presence of  
134 chemical groups onto the graphene basal plane. Lee et al.<sup>24</sup>

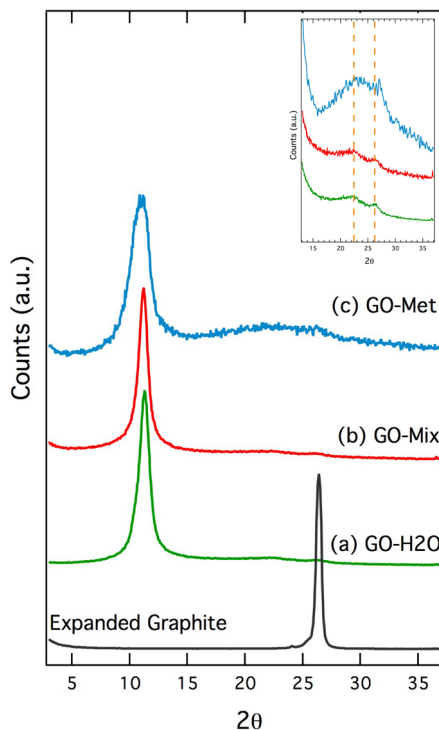


**Figure 1.** X-ray diffraction data for the GO dispersions: (a) GO-H<sub>2</sub>O, (b) GO-Mix, and (c) GO-Met. The peak at  $2\theta = 11.2^\circ$  identifies for GO. The spectrum of the expanded graphite is reported as a reference showing a sharp peak at  $2\theta = 26.5^\circ$ . Inset: the range 15–35° is expanded and shows two broad weak peaks at  $22.2^\circ$  and  $26.2^\circ$ .

attributed the broadness of the main peak to a certain amount of amorphous material coexisting with the crystalline phase. Moreover, the synthesis of graphene oxide implies the formation of GO flakes showing heterogeneous size distribution. Finally, the solubilization of GO in methanol leads to a not negligible amount of restacking graphene layers. All these factors, combined with the stochastic distribution of the GO flakes on the XRD sample holder, are concomitantly responsible for the observed broadening of the main peak. The main peak for GO samples is in agreement with the range of values of  $9^\circ$  and  $12^\circ$  reported in the literature.<sup>11,13,24–26</sup> Furthermore, the peak at around  $11^\circ$  was demonstrated to be correlated to a single GO layer by Dakin et al.<sup>27</sup> Similarly, Xu et al.<sup>28</sup> reported that the transition from graphite layers to graphene occurs with an interlayer distance greater than 0.424 nm ( $2\theta = 22^\circ$ ) using a scanning tunneling microscopy technique and DFT calculation. In addition to the main diffraction peak, a broad 15–35° peak is observed. Within this peak, we can distinguish two smaller peaks at  $22.2^\circ$  and  $26.2^\circ$  (Figure 1 inset). In general, these tiny peaks are not considered to be a characteristic signature for GO, and therefore they are often omitted from the X-ray spectra description. Nevertheless, they can be attributed to the presence of reduced graphene oxides in the powder mixture, as described by Shin et al.,<sup>29,30</sup> who studied the formation of reduced graphene oxides by increasing the amount of the reducing agent ( $\text{NaBH}_4$ ). Their work led to the observation of the formation of a broad peak at around  $23^\circ$  ( $d = 0.39 \text{ nm}$ , characteristic of multilayer graphene or unreacted graphite) and the progressive disappearance of the peak at  $10.7^\circ$  ( $d = 0.83 \text{ nm}$ ), characteristic of GO. In our experiments, the peak at  $26.2^\circ$  can be attributed either to expanded graphite or to multilayer graphene since the

167 interlayer distance for both peaks is  $d = 0.35$  nm, while the peak  
 168 at  $22.2^\circ$  according to the results of Shin<sup>29</sup> and Sun<sup>10</sup> results is  
 169 related to the formation of reduced graphene oxide.

170 The formation of GO dispersions is characterized by  
 171 different kinetics depending on the polarity of the solvent.  
 172 The fresh GO-Met dispersion appears as a totally clear yellow  
 173 solution, and GO-Mix and GO-H<sub>2</sub>O fresh dispersions appear  
 174 as darker suspensions with floating black particles (Figure 2)



**Figure 2.** Digital camera image of GO dispersed in methanol (left), in 1:1 methanol/water (middle), and in distilled water (right). From the top, GO dispersions after 5 min shaking (no sonication, waiting unshaken for 2 h), 7 days, and 50 days.

175 Top). After complete dispersion of the filtrate, a negligible  
 176 amount of precipitate is present in the GO-Met dispersion.  
 177 Conversely, the amount of precipitate increases with the water  
 178 content in the solvent. The best dispersibility may be due to the  
 179 lower polarity of methanol, whereby the interaction with the  
 180 hydrophobic basal plane of graphene is more favored. On the  
 181 contrary, in water dispersions, the hydrophobic GO basal plane  
 182 minimizes the interactions with water molecules forming  
 183 floating aggregates, as in surfactant solutions.<sup>31</sup> The amphiphilic  
 184 nature of the GO implies a limit of solubility (saturation)  
 185 according to the polarity of the solvent. The solubility for fresh  
 186 dispersions, when the GO is solubilized just after synthesis, can  
 187 be quantified in  $0.34 \pm 0.06$  g/L (GO-Met),  $0.2 \pm 0.04$  g/L  
 188 (GO-Mix), and  $0.18 \pm 0.04$  g/L (GO-H<sub>2</sub>O). On the  
 189 contrary, when GO is stored as a dry sample and then  
 190 dispersed in a polar solvent, the solubility appears to decrease  
 191 by about 35% in methanol and even 60% for water dispersions.

This discrepancy between the wet and dry GO material may 192 due to the degree of solvation of GO in the filtrate material. In 193 some cases, the solubility may appear to be higher if the 194 dispersion is not decanted (no less than 2 days) and the 195 saturation limit is reached. In fact, for water dispersions, 196 solubility may vary by up to 0.4 g/L in GO-H<sub>2</sub>O if floating 197 particles are also taken into account. After about 2–3 h, a 198 precipitate is found in the GO dispersions, and the supernatant 199 starts to appear as a clear amber solution. The color of the 200 supernatant is more intense in the water-containing dispersions 201 and is related to the presence of the conjugated systems in the 202 graphene basal plane. 203

**Functional Groups in GO Structure.** The solvent- 204 dependent functionalization of the graphene basal plane has 205 been investigated using Fourier-transformed infrared (FTIR) 206 spectroscopy. Figure 3 shows FTIR spectra for the GO 207 f3 dispersion (supernatant and precipitate) in methanol in the 0- 208 to-50-days time range. Spectra vary over time, indicating that 209 the chemical groups bonded to the graphene plane change 210 during the course of the dispersion and sedimentation 211

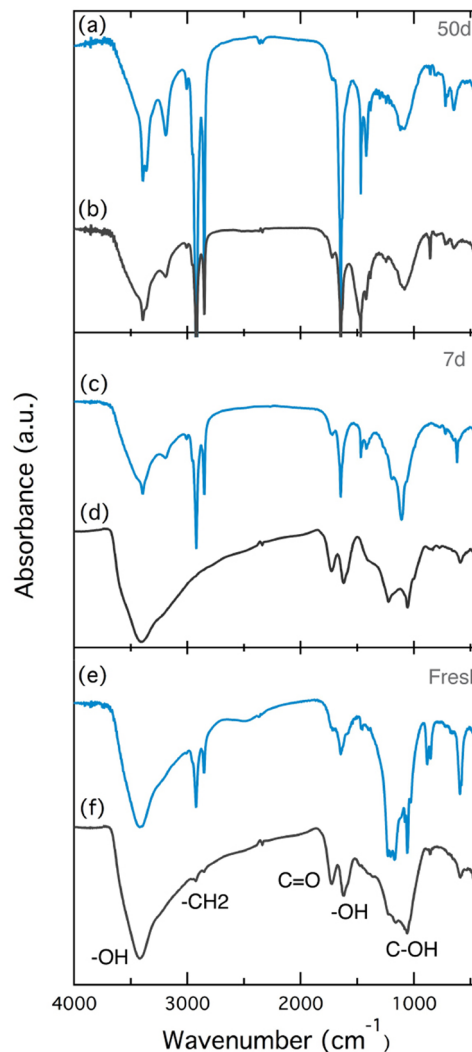


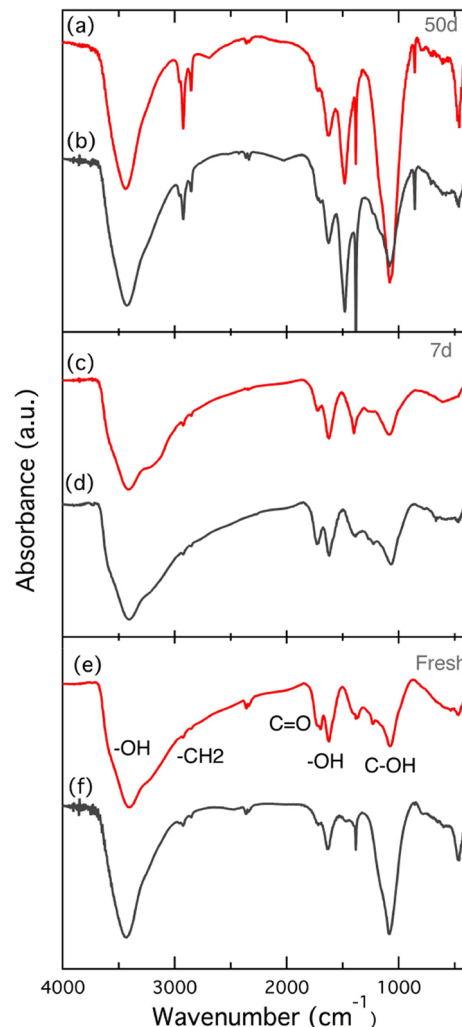
**Figure 3.** FTIR spectra for GO dispersed in MetOH, for fresh dispersion, after 7 days and 50 days. The colored plots (a, c, e spectra) correspond to the GO solubilized in the solvent (supernatant), while the gray plots (b, d, f, spectra) represent the corresponding GO GO

processes. Moreover, the spectra obtained from solid precipitate appear to be simpler than those from solvent dispersions, further suggesting a structural change. In all the spectra, the characteristic broad band of GO at  $3410\text{ cm}^{-1}$  corresponding to the stretching vibrations of bonded O–H remains clearly visible. The doublet peaks at 2920 and  $2850\text{ cm}^{-1}$  which correspond to the symmetric and antisymmetric stretching vibrations of  $-\text{CH}_2$  show an increase in intensity in going from fresh to 50-days dispersions and result in a stronger peak for the supernatant. The peak at  $1730\text{ cm}^{-1}$ , corresponding to the C=O stretching vibration, can also be found. Often, this band is attributed to the vibrations of the  $-\text{COOH}$  group.<sup>11,13,24–26,32</sup> The peak at  $1620\text{ cm}^{-1}$  is sometimes assigned to the O–H vibrations due to the presence of adsorbed water on the graphene basal plane.<sup>25</sup> Alternatively, these two peaks,  $1730$  and  $1620\text{ cm}^{-1}$ , can be interpreted as resulting from *keto–enol tautomerism*, an equilibrium known to occur in molecules carrying keto and enol groups. In our GO systems, the relative intensity of the peaks suggests that the tautomeric equilibrium shifts toward the enol form in all the solvents, while the two peaks maintain approximately the same intensity in the precipitate spectra. Furthermore, the scissoring vibrations of  $-\text{CH}_2$  are described by the doublet at 1468 and  $1417\text{ cm}^{-1}$  and disappear when the  $-\text{CH}_2$  stretching vibration peaks at 2920 and  $2850\text{ cm}^{-1}$  decrease. The shoulder around  $1375\text{ cm}^{-1}$  corresponds to the bending vibration of O–H. The stretching vibration for alcoholic C–OH in an aromatic six-membered ring shows at  $1228\text{ cm}^{-1}$ . The peak at  $1060\text{ cm}^{-1}$  has a controversial interpretation. Although some authors interpret this peak as the symmetric frequency referred to the epoxy group, it is more likely related to the stretching vibration of C–O for a primary alcohol. Generally, the interpretation of vibrations below  $1000\text{ cm}^{-1}$  is difficult and subject to several different interpretations. The doublet peaks  $850\text{ cm}^{-1}$ ,  $815\text{ cm}^{-1}$  and  $720\text{ cm}^{-1}$ ,  $645\text{ cm}^{-1}$  may correspond to the out-of-plane vibrations for C–H and O–H in an aromatic system and/or the rocking vibrations for C–H<sub>2</sub>.

Figure 4 shows the spectra for the GO–Mix dispersions. They have similar frequency groups as those observed in GO–Met spectra except for the presence of  $-\text{CH}_2$  doublet frequencies ( $2920$  and  $2850\text{ cm}^{-1}$ ). The intensity of the doublet is therefore drastically lowered when water is added to the dispersion.

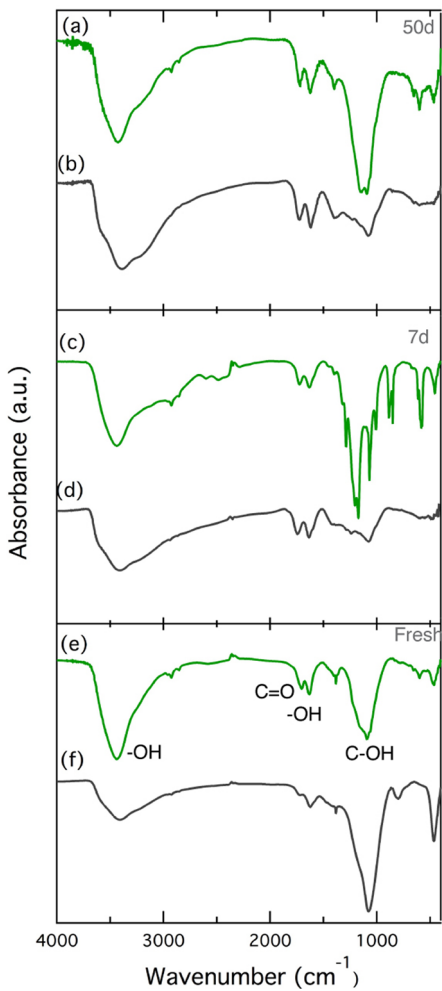
The GO–H<sub>2</sub>O FTIR spectra (Figure 5) exhibit comparable frequency groups of GO–Met, i.e., the broad band around  $3430\text{ cm}^{-1}$  for the stretching vibrations of O–H, the tautomeric equilibrium at 2920 and  $1620\text{ cm}^{-1}$ , and the band at  $1080\text{ cm}^{-1}$  for the stretching vibration of C–OH. However, some differences occur in the fingerprint region. In fresh dispersions (Figure 4e,f), a strong and broad band is found at around  $1080\text{ cm}^{-1}$  and may be attributed to the group frequency of C–OH and/or the presence of the epoxy group. This band appears broad for all fresh dispersions and becomes broader after 50 days. The region below  $900\text{ cm}^{-1}$  reveals bands mainly for the supernatant dispersions suggesting the presence of conjugated systems.

To investigate the presence of conjugated systems on the graphene basal plane, UV–vis experiments were performed on GO dispersed in polar solvents over a period of 50 days. As shown in Figure 6, the region 400–900 nm is not affected by absorptions. The difference between GO dispersions becomes apparent in the range 200–300 nm. In fresh GO–H<sub>2</sub>O dispersions, the maximum absorbance takes place at  $\lambda_{\text{Max}} = 230$



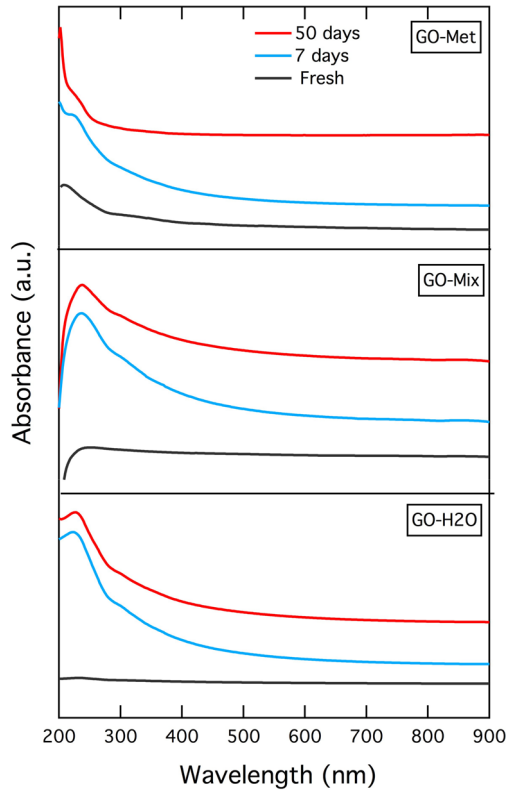
**Figure 4.** FTIR spectra for GO dispersed in 1:1 MetOH/H<sub>2</sub>O and for fresh dispersion, after 7 days and 50 days. The colored plots (a, c, e spectra) correspond to the GO solubilized in the solvent (supernatant), while the gray plots (b, d, f, spectra) represent the corresponding GO precipitate.

nm, while a slight decrease of about 5 nm is observed at maximum absorbance after 7 days and 50 days (see Table 2 in the Supporting Information (SI)). This is attributed to  $\pi \rightarrow \pi^*$  transitions in conjugated systems.<sup>32,33</sup> The intensity increases with time due to the formation of conjugated systems, as shown by FTIR results. A shoulder is present at around  $\lambda = 290\text{ nm}$  and is often attributed to the  $n \rightarrow \pi^*$  transition of a carbonyl group. This band is kinetically stable and shows a constant wavelength value of  $290\text{ nm}$ . A different spectrum profile is obtained with the GO–Mix dispersion. The fresh dispersion shows only a very tiny band at  $\lambda_{\text{Max}} = 240\text{ nm}$ . After 7 days, a distinct band appears at  $\lambda_{\text{Max}} = 238\text{ nm}$  with a shoulder at  $\lambda = 285\text{ nm}$ . Unlike GO–H<sub>2</sub>O, the spectra of GO–Met dispersions show a  $\lambda_{\text{Max}} = 205\text{ nm}$  and a shoulder at  $280\text{ nm}$ . The intensity of the maximum absorbance in the fresh dispersions is greater in methanol than in water dispersions, in agreement with the direct observation (see Figure 2). Upon GO–Met fresh dispersion formation, the UV–vis signal for the maximum of absorbance is shifted to shorter wavelengths ( $\lambda_{\text{Max}} = 202\text{ nm}$ ), and the shoulder has a  $\lambda$  around  $220\text{ nm}$ . Taking into account that the UV–vis cutoff of methanol for qualitative analysis is



**Figure 5.** FTIR spectra for GO dispersed in  $\text{H}_2\text{O}$  for fresh dispersion, after 7 days and 50 days. The colored plots (a, c, e spectra) correspond to the GO solubilized in the solvent (supernatant), while the gray plots (b, d, f, spectra) represent the corresponding GO precipitate.

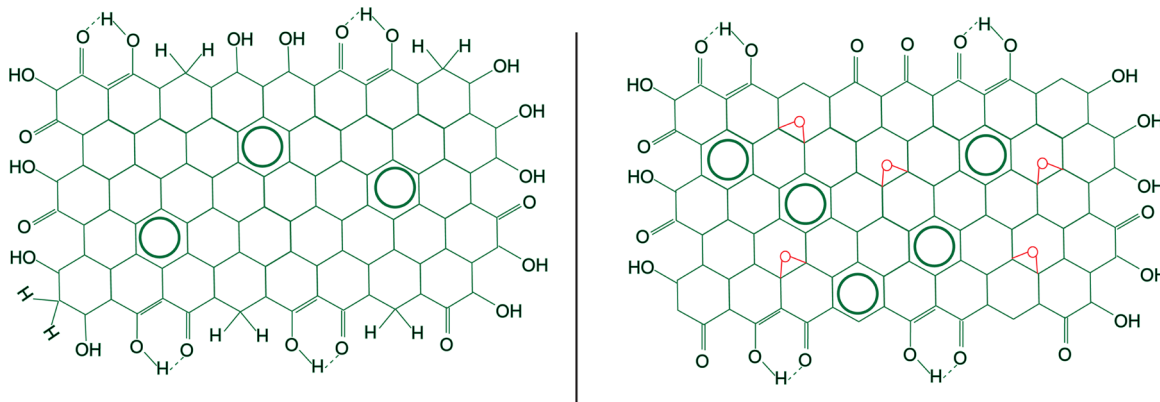
296 205 nm, any bands below this value are affected by solvent  
297 absorbance. Nevertheless, comparing GO-Met with GO-Mix  
298 and GO- $\text{H}_2\text{O}$  spectra, the shift of maximum absorbance from  
299 about 230 nm to about 205 nm can be attributed to the effect  
300 of the solvent. Actually, the polar solvent and the formation of  
301 hydrogen bonds have a more stabilizing effect on the  $\pi$  energy  
302 level than nonpolar solvents, thus causing a shift to longer  
303 wavelengths in the  $\pi \rightarrow \pi^*$  transitions, as shown for GO-Mix  
304 and GO- $\text{H}_2\text{O}$  dispersions. Moreover, the  $n \rightarrow \pi^*$  transitions  
305 are red-shifted because the carbonyl groups are part of a  
306 conjugated system. The UV-vis results suggest that more  
307 conjugated systems are present in water-containing dispersions  
308 than in methanol when GO is stored for a period longer than 7  
309 days in the liquid phase. This is in agreement with the FTIR  
310 conclusions. The GO-Met supernatant spectra (Figure 3)  
311 show a more intense peak at  $1620 \text{ cm}^{-1}$  which indicates that  
312 the keto-enol equilibrium is moved toward the enol form, thus  
313 reducing the number of aromatic systems. Even the peak at  
314  $1230 \text{ cm}^{-1}$  (frequency vibration for the Ar-OH group) is  
315 reduced with the time, and it can be correlated to the UV-vis  
316 spectra where the maximum absorbance is shifted to shorter  
317 wavelengths, indicating a reduction of the number of  
318 conjugated systems. Since the solvent affects the GO structure,  
319 a "self-functionalization" is likely to occur. The illustration in



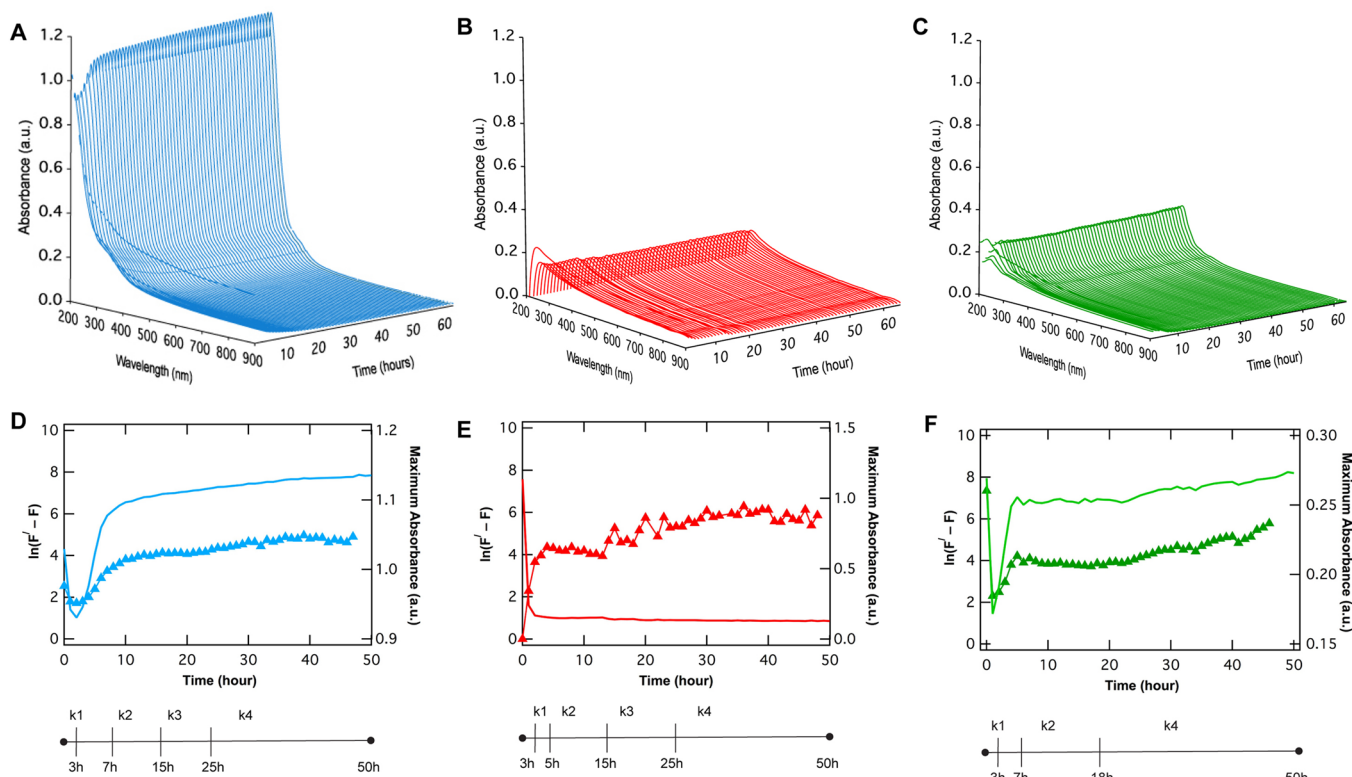
**Figure 6.** UV-vis spectra of the GO dispersed in  $\text{H}_2\text{O}$  (GO- $\text{H}_2\text{O}$ ), 1:1  $\text{H}_2\text{O}/\text{MetOH}$  (GO-Mix), and MetOH (GO-Met). The maximum absorbance peak is around 230 nm with a shoulder close to 300 nm.

Figure 7 helps the reader to schematize the modification of GO in methanol and water dispersions. 320 f7

**Kinetics of GO Solubilization.** The kinetic properties of 322 the solubilization/dispersion of GO in polar solvents are 323 evaluated from the 3D plots of the in situ UV-vis experiments, 324 which plot absorbance versus wavelength versus time. In Figure 325 f8 8A-C, the *in situ* UV-vis spectra show that the maximum 326 f8 absorbance corresponds to higher intensity when GO is 327 dispersed in methanol. This is consistent with our previous 328 observation that methanol helps the solubilization of GO. On 329 the other hand, the lower intensity of maximum absorbance in 330 the GO-Mix and GO- $\text{H}_2\text{O}$  dispersions provides evidence of 331 limited solubility. Besides, the intensity of UV-vis bands is not 332 only related to the amount of GO dispersed in the solvent but 333 also to the existence of conjugated systems within the GO 334 structure. In order to evaluate the kinetic parameters of GO 335 solubilization, maximum absorbance is plotted vs time, as 336 shown in Figure 8D-F (right, solid lines). Since floating 337 particles are present in solution at the very beginning of the 338 dispersion process, the UV-vis spectra show a higher  $\lambda_{\text{Max}}$  339 value than subsequent measurements. Hence, the first 2–3 h 340 from the beginning of the experiment have not been considered 341 because they do not univocally represent the actual 342 solubilization process. Concerning pure solvent dispersions, 343 the maximum absorbance tends to increase with time, smoothly 344 reaching a plateau after about 3 h. An opposite behavior is 345 obtained for GO-Mix dispersions, where the  $\lambda_{\text{Max}}$  decreases 346 until a plateau is reached. The kinetic constant can be evaluated 347 by means of the Guggenheim method<sup>34</sup> which conveniently 348 allows only part of the complete reaction to be considered 349



**Figure 7.** Schemes illustrating the alteration of graphene basal plane for GO dispersed in methanol (left) and water (right).



**Figure 8.** (A–C) *In situ* UV–vis measurements for the GO–Met (blue), GO–Mix (red), and GO–H<sub>2</sub>O (green) dispersions. (D–F) Corresponding maximum absorbance plots (right, solid lines) and Guggenheim function (left, dotted lines) versus time. Marks delineate each slope change. Kinetic parameters are reported in Table 4 in the SI.

without referring to the starting and ending points of the process. The Guggenheim method follows the equation:  $\ln(F' - F) = -kt + A$ , where  $k$  is the rate constant,  $t$  the time,  $R$  the gas constant,  $T$  the temperature,  $A$  a constant that can be considered as the Arrhenius prefactor,  $F'$  a property that is proportional to the concentration, and  $F$  the property  $F$  at a time  $(t + \Delta t)$ , where  $\Delta t$  is 2–3 half-life time. In our experiments  $F$  is the maximum absorbance for the *in situ* measurements. In Figure 8 is reported the  $\ln(F' - F)$  vs time (dotted lines). In general, behind 3 h it is difficult to precisely evaluate the kinetic constant because rather large floating particles, which can affect the quality of the signals, are dispersed in the solvent before precipitating. In the first slope, the Guggenheim function for GO–Met decreases during 5 h with a kinetic constant of  $0.37 \pm 0.03 \text{ h}^{-1}$ . In the same time

range, the  $k_1$  increases with the water content until  $0.6 \pm 0.05 \text{ h}^{-1}$  for pure water dispersion (GO–H<sub>2</sub>O), as shown in Table 4 in the SI. The higher value of  $k_1$  for GO dispersed in water may be related to the fact that oxygen domains show higher affinity to water molecules than to methanol. The second slope ( $k_2$ ) shows a distinct rate depending on the solvent. Between 7 and 20 h, a tiny negative  $k_2$  value is calculated for GO–H<sub>2</sub>O dispersions, which is evidence of the precipitation of GO, as shown by the direct observation in Figure 2. In the same time range, two distinct different slopes (both for  $k_2$  and  $k_3$ ) can be identified for GO–Met and GO–Mix dispersions. The  $k_2$  for the GO–Met dispersion is estimated in  $0.13 \pm 0.01 \text{ h}^{-1}$ , while it decreases to  $0.04 \pm 0.01 \text{ h}^{-1}$  for the GO–Mix dispersion. In the third slope, GO–Met and GO–Mix dispersions show a similar  $k_3$  value ( $0.008 \pm 0.004 \text{ h}^{-1}$ ). Also, the kinetic constant

<sup>380</sup>  $k_3$  is similar to  $k_1$ , except for GO–Mix dispersions, where  $k_3 =$   
<sup>381</sup>  $0.053 \pm 0.008 \text{ h}^{-1}$  and therefore is larger than  $k_1$ . Bearing in  
<sup>382</sup> mind that the Guggenheim method implies a linear fit only if  
<sup>383</sup> the process involves a single entity, the reaction rate of  
<sup>384</sup> dissolution can be evaluated from  $v = k[\text{GO}]$ . The  
<sup>385</sup> concentration of the initial  $\overline{\text{GO}}$  dispersions are calculated to  
<sup>386</sup> be  $1.9 \times 10^{-4} \text{ M}$  (GO–Met),  $1.0 \times 10^{-4} \text{ M}$  (GO–Mix), and  
<sup>387</sup>  $0.86 \times 10^{-4} \text{ M}$  (GO–H<sub>2</sub>O). Details about calculations of GO  
<sup>388</sup> concentration are reported in the SI. In the first slope, the pure  
<sup>389</sup> dispersions exhibit the same rate ( $v = 1.4 \times 10^{-8} \text{ mol L}^{-1} \text{ s}^{-1}$ ),  
<sup>390</sup> while a slower rate is observed for the mix dispersion (see  
<sup>391</sup> Table 4 in the SI). In the second slope, a moderate decrease in  
<sup>392</sup> the GO–Met rate is found. On the contrary, a negative rate is  
<sup>393</sup> calculated for GO–Mix and GO–H<sub>2</sub>O dispersions, which  
<sup>394</sup> indicates that GO is not solubilized in the solvent but a  
<sup>395</sup> precipitation occurs. After 15 h (third slope), a different  
<sup>396</sup> behavior is noticed in all GO dispersions. In GO–Met, the rate  
<sup>397</sup> ( $v = 4 \times 10^{-10} \text{ mol L}^{-1} \text{ s}^{-1}$ ) is slowed down. An opposite  
<sup>398</sup> behavior is observed from GO dispersed in the methanol/water  
<sup>399</sup> mixture, where, in fact, the rate becomes positive again  
<sup>400</sup> compared with the negative rate constante (precipitation) in  
<sup>401</sup> slope two. In the final slope, the rate is smaller for the methanol  
<sup>402</sup> dispersion ( $v = 1 \times 10^{-9} \text{ mol L}^{-1} \text{ s}^{-1}$ ), and it is comparable for  
<sup>403</sup> aqueous dispersions.

<sup>404</sup> The activation energy ( $E_a$ ) can be calculated from the  
<sup>405</sup> Arrhenius equation using the Guggenheim parameters in Table  
<sup>406</sup> 4 in the SI at room temperature. The  $E_a$  increases for each  
<sup>407</sup> slope, indicating that GO solubilization is more favored in the  
<sup>408</sup> first than in the last slope. A maximum increment of about 7 kJ  
<sup>409</sup> mol<sup>-1</sup> is observed in the *in situ* experiments during 50 h for  
<sup>410</sup> each dispersion. The activation energy of GO dissolution in  
<sup>411</sup> methanol is evaluated in  $1.2 \pm 0.9 \text{ kJ mol}^{-1}$   $\overline{\text{GO}}$  for the first  
<sup>412</sup> slope. This low value is in agreement with the spontaneous GO  
<sup>413</sup> solubilization in methanol, as can be seen from the direct  
<sup>414</sup> observation in Figure 2. When distilled water is used, the  $E_a$   
<sup>415</sup> increases to  $1.9 \pm 0.5 \text{ kJ mol}^{-1}$   $\overline{\text{GO}}$ , while a larger  $E_a$  is found  
<sup>416</sup> for GO–Mix. The alternative reaction route implies a higher  
<sup>417</sup> energy barrier GO has to overcome against the water  
<sup>418</sup> molecules. This reflects the trend seen for the reaction rate  
<sup>419</sup> (Table 4 in the SI), where  $v_1$  for mix dispersion is low  
<sup>420</sup> compared to pure solvent dispersions. Due to the GO  
<sup>421</sup> precipitation in GO–H<sub>2</sub>O and GO–Met dispersions, the  $E_a$   
<sup>422</sup> leads to higher barrier values close to  $24 \pm 3 \text{ kJ mol}^{-1}$   $\overline{\text{GO}}$ . In  
<sup>423</sup> the fourth slope,  $E_a$  has a magnitude of  $10 \text{ kJ mol}^{-1}$  suggesting  
<sup>424</sup> that GO reaches saturation and that any further GO  
<sup>425</sup> solubilization is possible which implies a higher energy barrier.

## CONCLUSIONS

<sup>426</sup> We showed that the structure and the solubilization kinetics of  
<sup>427</sup> GO are both affected by the solvent. GO can be described as a  
<sup>428</sup> basal plane of graphene decorated with hydroxyl and carbonyl  
<sup>429</sup> groups. The presence of  $-\text{CH}_2$  groups can be clearly  
<sup>430</sup> ascertained when methanol is used as solvent. The keto–enol  
<sup>431</sup> tautomerizm explains the presence of both hydroxyl ( $-\text{O}-\text{H}$ )  
<sup>432</sup> and carbonyl ( $-\text{C}=\text{O}$ ) groups, as well as the aromatic  
<sup>433</sup> character of the material. The presence of conjugated rings in  
<sup>434</sup> the GO structure has been further confirmed also by UV–vis  
<sup>435</sup> spectral analysis. Structural changes have an impact on the  
<sup>436</sup> material's dispersion rate, which decreases by about 1 order of  
<sup>437</sup> magnitude between the first and last slope due to the specific  
<sup>438</sup> functional groups that are present on the graphene basal plane.  
<sup>439</sup> Furthermore, the solubility of the material varies depending on

the solvent, the lower polarity of methanol providing a better  
<sup>440</sup> GO dispersion than water. In fact, in methanol GO overcomes  
<sup>441</sup> a lower activation energy than in water solutions, where a larger  
<sup>442</sup> amount of precipitate is present. Thus, we proved that the GO  
<sup>443</sup> dispersions are not stable solutions, but they are sensitive to the  
<sup>444</sup> polar solvent used. Finally, we argue that the GO can not be  
<sup>445</sup> treated as simple derivated graphene material made by carbon  
<sup>446</sup> and oxygen atoms but rather as a complex system where the  
<sup>447</sup> extent and the nature of the functionalization depend on several  
<sup>448</sup> factors including the solvent and the aging status.  
<sup>449</sup>

## ASSOCIATED CONTENT

### S Supporting Information

SEM images, FTIR frequency table, and UV band table. This  
<sup>453</sup> material is available free of charge via the Internet at <http://pubs.acs.org>.  
<sup>454</sup>  
<sup>455</sup>

## AUTHOR INFORMATION

### Corresponding Author

\*E-mail: flavio.pendolino@unipd.it.  
<sup>457</sup>  
<sup>458</sup>

### Notes

The authors declare no competing financial interest.  
<sup>459</sup>  
<sup>460</sup>

## ACKNOWLEDGMENTS

This work was supported by the University of Padova under  
<sup>462</sup> “Progetto Strategico MAESTRA”. E.P. acknowledges the  
<sup>463</sup> European Union for financial support (Marie Curie FP7 IRG  
<sup>464</sup> grant N. 268231).  
<sup>465</sup>

## REFERENCES

- (1) Compton, O. C.; Nguyen, S. T. Graphene Oxide, Highly Reduced Graphene Oxide, and Graphene: Versatile Building Blocks for Carbon-Based Materials. *Small* **2010**, *6*, 711–723.  
<sup>467</sup>  
<sup>468</sup>
- (2) Su, C.; Loh, K. P. Carbocatalysts: Graphene Oxide and Its Derivatives. *Acc. Chem. Res.* **2012**, *46*, 2275–2285.  
<sup>470</sup>  
<sup>471</sup>
- (3) Lerf, A.; He, H.; Forster, M.; Klinowski, J. Structure of Graphite Oxide Revisited. *J. Phys. Chem. B* **1998**, *102*, 4477–4482.  
<sup>472</sup>  
<sup>473</sup>
- (4) He, H. Y.; Klinowski, J.; Forster, M.; Lerf, A. A new structural model for graphite oxide. *Chem. Phys. Lett.* **1998**, *287*, 53–56.  
<sup>474</sup>  
<sup>475</sup>
- (5) Dreyer, D. R.; Todd, A. D.; Bielawski, C. W. Harnessing the chemistry of graphene oxide. *Chem. Soc. Rev.* **2014**, *43*, 5288–5301.  
<sup>476</sup>  
<sup>477</sup>
- (6) Hofmann, U.; König, E. Untersuchungen über Graphitoxyd. Z. Anorg. Allg. Chem. **1937**, *234*, 311–336.  
<sup>478</sup>  
<sup>479</sup>
- (7) Hummers, W. S., Jr.; Offeman, R. E. Preparation of Graphitic Oxide. *J. Am. Chem. Soc.* **1958**, *80*, 1339–1339.  
<sup>480</sup>  
<sup>481</sup>
- (8) Brodie, B. C. On the Atomic Weight of Graphite. *Philos. Trans. R. Soc. London* **1859**, *149*, 249–259.  
<sup>482</sup>  
<sup>483</sup>
- (9) Marcano, D. C.; Kosynkin, D. V.; Berlin, J. M.; Sinteskii, A.; Sun, Z.; Slesarev, A.; Alemany, L. B.; Lu, W.; Tour, J. M. Improved Synthesis of Graphene Oxide. *ACS Nano* **2010**, *4*, 4806–4814.  
<sup>484</sup>  
<sup>485</sup>
- (10) Sun, L.; Fugetsu, B. Mass production of graphene oxide from expanded graphite. *Mater. Lett.* **2013**, *109*, 207–210.  
<sup>487</sup>  
<sup>488</sup>
- (11) Dimiev, A. M.; Tour, J. M. Mechanism of Graphene Oxide Formation. *ACS Nano* **2014**, *8*, 3060–3068.  
<sup>489</sup>  
<sup>490</sup>
- (12) Higginbotham, A. L.; Kosynkin, D. V.; Sinteskii, A.; Sun, Z.; Tour, J. M. Lower-Defect Graphene Oxide Nanoribbons from Multiwalled Carbon Nanotubes. *ACS Nano* **2010**, *4*, 2059–2069.  
<sup>491</sup>  
<sup>492</sup>
- (13) Yeh, T.-F.; Syu, J.-M.; Cheng, C.; Chang, T.-H.; Teng, H. Graphite Oxide as a Photocatalyst for Hydrogen Production from Water. *Adv. Funct. Mater.* **2010**, *20*, 2255–2262.  
<sup>494</sup>  
<sup>495</sup>
- (14) Xu, J.; Wang, K.; Zu, S.-Z.; Han, B.-H.; Wei, Z. Hierarchical Nanocomposites of Polyaniline Nanowire Arrays on Graphene Oxide Sheets with Synergistic Effect for Energy Storage. *ACS Nano* **2010**, *4*, 499 5019–5026.  
<sup>497</sup>  
<sup>498</sup>  
<sup>499</sup>  
<sup>500</sup>

- 501 (15) Cote, L. J.; Kim, J.; Tung, V. C.; Luo, J.; Kim, F.; Huang, J.  
502 Graphene oxide as surfactant sheets. *Pure Appl. Chem.* **2011**, *83*, 95–  
503 110.
- 504 (16) Liu, Y.; Yu, D.; Zeng, C.; Miao, Z.; Dai, L. Biocompatible  
505 graphene oxide-based glucose biosensors. *Langmuir* **2010**, *26*, 6158–  
506 6160.
- 507 (17) Ariffin, S. N.; Lim, H. N.; Jumeri, F. A.; Zobir, M.; Abdullah, A.  
508 H.; Ahmad, M.; Ibrahim, N. A.; Huang, N. M.; Teo, P. S.;  
509 Muthoosamy, K.; Harrison, I. Modification of polypropylene filter  
510 with metal oxide and reduced graphene oxide for water treatment.  
511 *Ceram. Int.* **2014**, *40*, 6927–6936.
- 512 (18) Perreault, F.; Tousley, M. E.; Elimlech, M. Thin-Film  
513 Composite Polyamide Membranes Functionalized with Biocidal  
514 Graphene Oxide Nanosheets. *Environ. Sci. Technol. Lett.* **2014**, *1*,  
515 71–76.
- 516 (19) Si, Y.; Samulski, E. T. Synthesis of water soluble graphene. *Nano*  
517 *Lett.* **2008**, *8*, 1679–1682.
- 518 (20) Kim, J.; Cote, L. J.; Huang, J. Two Dimensional Soft Material:  
519 New Faces of Graphene Oxide. *Acc. Chem. Res.* **2012**, *45*, 1356–1364.
- 520 (21) Stankovich, S.; Piner, R. D.; Chen, X.; Wu, N.; Nguyen, S. T.;  
521 Ruoff, R. S. Stable aqueous dispersions of graphitic nanoplatelets via  
522 the reduction of exfoliated graphite oxide in the presence of  
523 poly(sodium 4-styrenesulfonate). *J. Mater. Chem.* **2006**, *16*, 155–155.
- 524 (22) Eigler, S.; Grimm, S.; Hof, F.; Hirsch, A. Graphene oxide: a  
525 stable carbon framework for functionalization. *J. Mater. Chem. A* **2013**,  
526 *1*, 11559–11562.
- 527 (23) Schlierf, A.; Yang, H.; Gebremedhn, E.; Treossi, E.; Ortolani, L.;  
528 Chen, L.; Minoia, A.; Morandi, V.; Samori, P.; Casiraghi, C.; et al.  
529 Nanoscale insight into the exfoliation mechanism of graphene with  
530 organic dyes: effect of charge, dipole and molecular structure.  
531 *Nanoscale* **2013**, *5*, 4205–4216.
- 532 (24) Lee, D. W.; De Los Santos, L. V.; Seo, J. W.; Felix, L. L.;  
533 Bustamante D, A.; Cole, J. M.; Barnes, C. H. W. The Structure of  
534 Graphite Oxide: Investigation of Its Surface Chemical Groups. *J. Phys.*  
535 *Chem. B* **2010**, *114*, 5723–5728.
- 536 (25) Kaniyoor, A.; Baby, T. T.; Ramaprabhu, S. Graphene synthesis  
537 via hydrogen induced low temperature exfoliation of graphite oxide. *J.*  
538 *Mater. Chem.* **2010**, *20*, 8467–8469.
- 539 (26) Shen, B.; Lu, D.; Zhai, W.; Zheng, W. Synthesis of graphene by  
540 low-temperature exfoliation and reduction of graphite oxide under  
541 ambient atmosphere. *J. Mater. Chem. C* **2013**, *1*, 50–53.
- 542 (27) Dikin, D. a.; Stankovich, S.; Zimney, E. J.; Piner, R. D.;  
543 Dommett, G. H. B.; Evmenenko, G.; Nguyen, S. T.; Ruoff, R. S.  
544 Preparation and characterization of graphene oxide paper. *Nature*  
545 **2007**, *448*, 457–460.
- 546 (28) Xu, P.; Yang, Y.; Barber, S. D.; Schoelz, J. K.; Qi, D.; Ackerman,  
547 M. L.; Bellaiche, L.; Thibado, P. M. New scanning tunneling  
548 microscopy technique enables systematic study of the unique  
549 electronic transition from graphite to graphene. *Carbon* **2012**, *50*,  
550 4633–4639.
- 551 (29) Shin, H.-J.; Kim, K. K.; Benayad, A.; Yoon, S.-M.; Park, H. K.;  
552 Jung, I.-S.; Jin, M. H.; Jeong, H.-K.; Kim, J. M.; Choi, J.-Y.; Lee, Y. H.  
553 Efficient Reduction of Graphite Oxide by Sodium Borohydride and Its  
554 Effect on Electrical Conductance. *Adv. Funct. Mater.* **2009**, *19*, 1987–  
555 1992.
- 556 (30) Jung, H.; Yang, S. J.; Kim, T.; Kang, J. H.; Park, C. R. Ultrafast  
557 room-temperature reduction of graphene oxide to graphene with  
558 excellent dispersibility by lithium naphthalenide. *Carbon* **2013**, *63*,  
559 165–174.
- 560 (31) Jalili, R.; Aboutalebi, S. H.; Esrafilzadeh, D.; Konstantinov, K.;  
561 Razal, J. M.; Moulton, S. E.; Wallace, G. G. Formation and  
562 processability of liquid crystalline dispersions of graphene oxide.  
563 *Mater. Horiz.* **2013**, *1*, 87–91.
- 564 (32) Cao, H.; Wu, X.; Yin, G.; Warner, J. H. Synthesis of Adenine-  
565 Modified Reduced Graphene Oxide Nanosheets. *Inorg. Chem.* **2012**,  
566 *51*, 2954–2960.
- 567 (33) Paredes, J. I.; Villar-Rodil, S.; Martínez-Alonso, A.; Tascón, J. M.  
568 D. Graphene oxide dispersions in organic solvents. *Langmuir* **2008**, *24*,  
569 10560–10564.
- (34) Guggenheim, E. A. XLVI. On the determination of the velocity 570  
constant of a unimolecular reaction. *Philos. Mag.* **1926**, *2*, 538–543. 571